NUMERICAL INVESTIGATIONS OF THE STEADY STATE RELATIVE PERMEABILITY FUNCTIONALITY

Kåre Langaas, RF-Rogaland Research, Norway
Paul Papatzacos, Stavanger College, Norway

Abstract

The purpose of this paper is to investigate, by flow simulations in a uniform pore-space geometry, how the co- and countercurrent steady state relative permeabilities depend on the following parameters: phase saturation, wettability, driving force and viscosity ratio.

The main results are as follows: (i) with few exceptions, relative permeabilities are convex functions of saturation; (ii) the cocurrent relative permeabilities increase while the countercurrent ones decrease with the driving force; (iii) with some exceptions, phase 2 relative permeabilities decrease and phase 1 relative permeabilities increase with the viscosity ratio $M = \mu_1/\mu_2$; (iv) the countercurrent relative permeabilities are always less than the cocurrent ones, the difference being partly due to the opposing effect of the viscous coupling, and partly to different levels of capillary forces; (v) the pore-level saturation distribution, and hence the size of the viscous coupling, can be very different between the cocurrent and the countercurrent cases so that it is in general incorrect to estimate the full mobility tensor from cocurrent and countercurrent steady state experiments, as suggested by Bentsen and Manai [1].

Introduction

One-dimensional two-phase flow in porous media is usually assumed to follow the"conventional" extension of Darcy's law

$$\bar{u}_i = \lambda_i F_i. \tag{1}$$

where $\bar{u}_i$ is the Darcy velocity, λ_i the mobility, and F_i the driving force of phase i, $i = 1, 2$. The mobility is usually decomposed as $\lambda_i \equiv (kk_{ri})/\mu_i$ where k is the absolute permeability, k_{ri} the "conventional" relative permeability of phase i and μ_i the viscosity of phase i. The driving force consists of a pressure gradient term and a gravity term for each phase. The relative permeabilities are usually assumed to be functions of saturation only [2].

A modification of this flow law includes terms which account for the viscous drag of one fluid on the other [3, 4]

$$\bar{u}_i = \sum_{j=1}^{2} \lambda_{ij} F_j. \tag{2}$$

To estimate the four mobilities that enter this "general" Darcy law it is common to conduct two types of flow experiments.

Thus Rothman *et al.* [5, 6, 7] use two sets of numerical simulations, alternatively forcing just one of the phases: simulations with $F_1 \neq 0$, $F_2 = 0$ (or $F_1 = 0$, $F_2 \neq 0$) determine λ_{11} and λ_{21} (or λ_{12} and λ_{22}).

Noting that Eq. 2 reduces to Eq. 1 when the driving forces are equal or opposite ($F_1 = +F_2$ implies $\lambda_i^+ = \sum_{j=1}^{2} \lambda_{ij}$ while $F_1 = -F_2$ implies $\lambda_i^- = \sum_{j=1}^{2}(2\delta_{ij} - 1)\lambda_{ij}$ where δ_{ij} is the Kronecker delta) Bentsen and Manai [1] determine the λ_i^+ through equal forcing and the λ_i^- through opposite forcing steady state experiments.

For the calculation of the full mobility-tensor, both procedures must assume that the λ_{ij} are independent of the flow type. To avoid this assumption Avraam and Payatakes [8] have proposed a method to estimate the λ_{ij} from a single experiment using an inverse method. Inverse problems, however, are ill-posed.

If the general mobilities λ_{ij} are process-independent and have the same value when one or both phases are forced, the results of Rothman *et al.* imply that the equal forcing cocurrent and countercurrent mobilities are roughly independent of the driving force above the percolation threshold.

Experiments with cocurrent steady state flow in a uniform micromodel [9] have shown, however, that the conventional relative permeabilities may increase by a factor of 5 to 10, when the capillary number is increased by a factor of 15.

The impact of the viscosity ratio on the cocurrent relative permeabilities have been investigated earlier by several authors. The numerical (unsteady state) investigations of Goode and Ramakrishnan [10] are consistent with earlier experiments [11], showing that the non-wetting phase (phase 2) relative permeability is a decreasing function, while the wetting phase (phase 1) relative permeability is a weak function of $M = \mu_1/\mu_2$. The steady state cocurrent micromodel experiments of Avraam and Payatakes [9] show that both relative permeabilities decrease with increasing M, although less for the wetting phase when compared to the non-wetting phase.

The intention of this paper is to study the functionality of both the equal forcing cocurrent and the opposite forcing countercurrent steady state relative permeabilities in a uniform pore-space geometry. The functionality of the countercurrent relative permeability with respect to wettability, applied force and viscosity ratio have not, to our knowledge, been investigated earlier. To study the countercurrent flow is itself of practical interest, as it reflects the flow happening under *e.g.* gravity segregation.

Numerical method

We simulate the flow of two immiscible phases on the pore scale by a "first principles" two-dimensional (2D) model. A thermodynamically consistent lattice Boltzmann model of a binary fluid is used. The model simulates the Navier-Stokes equation for the total density and the convection-diffusion equation for the density-difference between the components, see Refs. [12, 13] for details. Different phase viscosities [14] and a general wettability description through "background chemical potential"(WP) [15] are included. We consider a neutrally wet ($WP = 0$) and a phase-1 wet ($WP = 0.05$) system. (The internodal distance Δx, the time step Δt and the mass unit are set equal to 1 when referring to variables and parameters of the method). The approach has been extensively verified [16, 14, 17] and the lattice Boltzmann parameters used here are the same as in Refs. [15, 17]. In particular, the surface tension parameter κ is 0.04 giving a theoretical surface tension $\sigma = 0.04428$ [16].

To avoid end-effects periodic boundary conditions are used. The flow is driven by a component-specific body force $\mathbf{F} = n * (\mathbf{g_A} x_A + \mathbf{g_B} x_B)$, where n is the total density (=2 in the bulk phases), x_A and x_B are the fractions of component A and B, while $\mathbf{g_A}$ and $\mathbf{g_B}$ are the body-forces on components A and B.

Numerical experiment setup

The porous medium is a square lattice with 288 nodes in each of two orthogonal direction identified below as $\mathbf{i}_X$ and $\mathbf{i}_Y$. Flow takes place in the space between 64 regularly distributed identical obstacles (sand grains). Each obstacle is an octagon made by cutting the corners of a 24×24 square in such a way that the length of the sides parallel to $\mathbf{i}_X$ or $\mathbf{i}_Y$ is 12; the length of the remaining sides is then $6\sqrt{2}$. See the blank space in Fig. 1 (left). The centers of the octagons occupy the sites $18(2n+1)\mathbf{i}_X + 18(2m+1)\mathbf{i}_Y$, $(m, n = 0, \ldots, 7)$. The diameter of that part of a "pore" which is parallel to $\mathbf{i}_X$ or $\mathbf{i}_Y$ is 12.

The driving force on phase i is $\mathbf{F_i} = n\mathbf{G_i}$. In all the simulations reported in this paper, $\mathbf{G_1} = \mathbf{G_2} = G(\mathbf{i}_X + \mathbf{i}_Y)$ for cocurrent flow, and $\mathbf{G_1} = -\mathbf{G_2} = G(\mathbf{i}_X + \mathbf{i}_Y)$ for countercurrent flow.

To determine the absolute permeability of this system, it is sufficient to simulate one-phase flow around one obstacle using periodic boundary conditions. The steady state velocity field is shown in Fig. 1 (left). The absolute permeability (calculated as the averaged x-component of velocity divided by G and multiplied by the viscosity) is shown on Fig. 1 (right). Deviations from Darcy's law, due to the increased importance of the inertial terms in the Navier-Stokes equation [18], are seen to be small: the absolute permeabilities at $G = 10^{-5}$ and $G = 10^{-3}$ are respectively $\sim 0.05\%$ higher and $\sim 3.80\%$ lower than the absolute permeability at $G = 10^{-4}$.

The initial state of the fluid, for all two-phase simulations reported in this paper, is a mixture of the two phases: at each grid cell fluid is randomly generated as either phase 1 or phase 2 (bulk values) with a probability equal to the desired saturation. Phase separation under flow will determine the saturation distribution at steady state. The cocurrent flow saturation distributions in the neutrally wet system at early times are shown in Fig. 2. The plot is a density-plot of the density difference parameter. Bulk phase 1 is white, bulk phase 2 is black and the obstacles are gray. Time step 0 (left) shows the initial state. One can see from the interface curvatures (middle and right figures) that the overall flow direction is along $\mathbf{i}_X + \mathbf{i}_Y$ (up-right on the figure). The specific randomization at the initial state turns out not to be important for the steady state flow properties. However, to ensure that different initial conditions do not bias the subsequent calculations, the same initial condition is used in all simulations having the same phase saturation.

The relative permeabilities presented below are calculated from the steady state Darcy velocities by the following procedure. The space-averaged velocity components are calculated at every 100 time step (for phase 1, phase 2, and total) and plotted versus time. Fig. 3 shows the x- and y-component of the total velocity for the cocurrent neutral wet case. In all cases, steady state is reached at a time step of approximately 50000. We then use a steady state period of typically 60000 steps to calculate mean values and standard deviations (x and y components are lumped together). The resulting standard deviations on the relative permeabilities are illustrated in the plots by error bars extending one standard deviation above and one below the mean value.

The results presented below show how the cocurrent and the countercurrent flow, both in a neutrally wet and a phase 1-wet system, vary with the saturation of phase 1 (S), the level of forcing (G) and the viscosity ratio (M).

The base case, for either cocurrent or countercurrent, is defined by $S = 0.5$, $G = 10^{-4}$, and $\mu_1 = \mu_2 = 1/3$.

Results

Effect of phase saturation

Neutrally wet: Figure 4 shows steady state cocurrent flow in the neutrally wet system. At $S = 0.25$ (left figure) phase 1 travels as "ganglions" [9] of different sizes through the system. The surface tension tries to minimize the interface between the phases. This capillary resistance will make the total flow rate smaller than in the one-phase case. At $S = 0.5$ (right figure) the phase distribution is symmetric as it should be. The two phases travel as ganglions, but these have a tendency to form clusters long in the direction orthogonal to the flow direction. Due to the larger interface at $S = 0.5$, one expect the flow to be more reduced due to capillary resistance, as compared to $S = 0.25$. This is shown in the relative permeabilities in Fig. 8 (left). The situation at $S = 0.75$ is expected to be phase-symmetric to that at $S = 0.25$ and this point on the relative permeability curve is taken from the calculations at $S = 0.25$.

The countercurrent steady state situations are shown in Fig. 5. Due to the opposite drag from phase 2, phase 1 is almost immobile at $S = 0.25$ (left figure). At $S = 0.5$ (right figure) most of phase 1 travels in the $\mathbf{i}_X + \mathbf{i}_Y$ direction while most of phase 2 travels in the opposite direction. Both phases are close to establishing connected channels. The capillary resistance is expected to be lower as compared to the cocurrent case due to the lower interfacial area. However, due to the negative drag of the other phase, the countercurrent relative permeabilities are lower than the cocurrent ones at $S = 0.5$, see Fig. 8 (left). For the countercurrent curves, the point at $S = 0.75$ is estimated by symmetry considerations.

The few points calculated for the neutrally wet system indicate that the countercurrent relative permeabilities are convex functions of saturation. The cocurrent curves seem to have a convex part at intermediate saturations only.

Phase 1-wet: Figure 6 shows the steady state cocurrent flow in the phase 1-wet system. At $S = 0.25$ (left figure) phase 1 is almost immobile, trapped by the wetting surfaces. At $S = 0.5$ (middle figure) both phases are connected. The fluid particles may travel in these connected channels,

but there is still motion of the interface through "finger" evolution and drop flow of phase 2. At $S = 0.75$ (right) phase 2 travels as drops.

The countercurrent steady state situations are shown in Fig. 7. Again phase 1 seems to be immobile at $S = 0.25$ (left figure), but the "tail" of these trapped units is now pointing in the opposite direction when compared to the cocurrent case, due to the opposite viscous drag. At $S = 0.5$ (middle figure) the non-wetting phase 2 has formed a connected network, while the wetting phase has not. As a consequence, the flow of phase 1 is close to immobile. At $S = 0.75$ (right figure) most of the phase 2 drops/ganglions are immobile.

The relative permeabilities are shown in Fig. 8 (right). All of them are convex functions of saturation.

Effect of driving force

Neutrally wet: Figure 9 shows the phase distribution for cocurrent steady state flow in the neutrally wet system at various force levels. The $G = 10^{-4}$ case is shown in Fig. 4 (right). With $G \leq 10^{-4}$ each phase travels as small and large ganglions, where the large ones are long only in the direction orthogonal to the flow. This kind of transport will be greatly affected by the surface tension. At $G = 2\,10^{-4}$ the two phases segregate and form more or less stationary channels along the flow direction. This saturation distribution survives when G is increased to 10^{-3}, but the channels are now typically thinner. When the phases are distributed as stationary channels along the flow direction, the surface tension does not significantly affect the flow, and a total flow rate similar to the one-phase situation is expected. This change in the microscopic phase distribution makes the cocurrent relative permeabilities (at $S = 0.5$) to jump from a value ~ 0.2 in the ganglion regime to a value ~ 0.5 in the stationary channel regime, see Fig. 13 (left).

Figure 10 shows the phase distribution at countercurrent steady state flow in the neutrally wet system. The $G = 10^{-4}$ situation is shown in Fig. 5 (right). At $G \leq 10^{-4}$ the size of the ganglions is relatively large. An increase in the driving force is seen to create smaller phase units and a larger interfacial area. Consequently, the capillary resistance will increase with increasing G, which is the opposite of the cocurrent result. Also the viscous coupling increases with increasing interface, and as a result the countercurrent relative permeabilities decrease somewhat faster than linearly as functions of the applied force, see Fig. 13 (left).

Note that the countercurrent relative permeabilities are always less than the cocurrent relative permeabilities. The ratio between the two becomes less with increasing forcing and is only 13.3% at the highest driving force investigated. Also, the time fluctuations (indicated by the error bars) are larger for the countercurrent flow.

Phase 1-wet: The cocurrent steady state flows in the phase 1-wet system at various levels of forcing are shown in Fig. 11. The $G = 10^{-4}$ case is shown in Fig. 6 (middle). At $G \leq 2\,10^{-4}$ (Fig. 11, left and middle) the non-wetting phase 2 travels as large ganglions which may form a connected network. More or less stationary channels along the flow direction are formed at $G = 5\,10^{-4}$ (right figure). The stationary channels become thinner as the driving force is increased further. Thus the shift from a ganglion regime to a stationary channel regime happens at a higher driving force for the wetting system as compared to the neutrally wet system. As in the case of the neutrally wet cocurrent case, the capillary forces are reduced with increasing driving force, and a total flow rate similar to the 1-phase situation is expected at the high-level forcing. Except for a tendency to decrease in the interval from $G = 5\,10^{-4}$ to $G = 10^{-3}$ for the wetting phase, both cocurrent relative permeabilities increase almost linearly with the applied force, see Fig. 13 (right). In particular, there is no jump in the relative permeabilities even though the saturation distribution changes when passing from $G = 2\,10^{-4}$ to $G = 5\,10^{-4}$.

Figure 12 shows the countercurrent steady state flow in the phase 1-wet system at various levels of forcing. The $G = 10^{-4}$ case is shown in Fig. 7 (middle). At all levels of forcing the flow regime is more or less stationary channel flow. For low-level forcing ($G \leq 10^{-4}$) these channels are not aligned with the driving force, but parallel to $\mathbf{i}_X$ or $\mathbf{i}_Y$. Some of the non-wetting phase is trapped as

immobile drops. At $G \geq 2\,10^{-4}$, the non-wetting network aligns with the flow direction and becomes thinner with an increased interfacial area. Looking at the countercurrent curves in Fig. 13 (right), the non-wetting relative permeability is seen to decrease as a function of the applied force, except at $G < 10^{-4}$. The wetting relative permeability is low (~ 0.05) and close to constant.

Effect of viscosity ratio

We now look at the effect of the viscosity ratio, M. In addition to the $M = 1$ case already investigated using $\mu_1 = \mu_2 = 1/3$, cases with $M = 0.1$ and $M = 10$ are investigated, using $\mu_1 = 1/15$ for $M = 0.1$ and $\mu_2 = 1/15$ for $M = 10$.

Neutrally wet: Figure 14 (left) shows the cocurrent steady state flow in the neutrally wet system with $M = 0.1$. The corresponding $M = 1$ case is shown in Fig. 4 (right). The low-viscosity phase 1 (white) has formed a broad channel, and the high-viscosity phase 2 is close to being connected. The reason for the better ability of phase 1 to produce channels is probably due to the fingering tendency of low viscosity phases in general. It is possible to see some phase 1 fingers on the figure. Even though phase 2 has twice the viscosity of the base case, its Darcy velocity is almost 3 times higher than in the base case. This is partly due to the phase distribution being more aligned along the flow direction, which causes less capillary resistance, but the main reason is probably the lubrication by the less-viscous phase 1. The strong viscous coupling between the phases is also the reason why the phase 1 Darcy velocity is not more than ~ 1.7 times the phase 2 velocity. This makes the relative permeability of phase 2 at $M = 0.1$ larger than unity, see Fig. 17 (left). The relative permeability at $M = 10$ is estimated by considerations of symmetry. The calculations indicate that the cocurrent relative permeabilities are convex functions of M.

The countercurrent steady state flow with $M = 0.1$ is shown in Fig. 14 (right). The corresponding $M = 1$ case is shown in Fig. 7 (right). The phase distribution is not very different from the cocurrent case, with phase 1 having the best channels. The phase 1 Darcy velocity is ~ 5.6 times that of phase 2, giving a phase 2 relative permeability ~ 2 times that of phase 1, see Fig. 17 (left). The relative permeability at $M = 10$ is estimated by considerations of symmetry. The calculations indicate that the countercurrent relative permeabilities are much less influenced by the viscosity ratio than the cocurrent ones.

Phase 1-wet: Figure 15 shows the cocurrent steady state flow situations in the phase 1-wet system having $M = 0.1$ and $M = 10$. The corresponding $M = 1$ case is shown in Fig. 6 (middle). At $M = 0.1$ the low-viscosity phase 1 covers the walls, some places as a thin film, thus lubricating the flow of the high-viscosity phase 2. As a result, the relative permeability of phase 2 gets far above unity (~ 1.7), see Fig. 17 (right). At $M = 10$ the wetting phase is that of high viscosity, providing a much poorer lubrication to the flow of phase 2. Both relative permeability curves seem to be convex functions of M, but it is clear that M has the largest effect on the non-wetting phase, see Fig. 17 (right). In particular, the cocurrent non-wetting relative permeability is ~ 13 times higher at $M = 0.1$ as compared to $M = 10$.

The countercurrent cases at $M = 0.1$ and $M = 10$ are shown in Fig. 16. The corresponding $M = 1$ case is shown in Fig. 7 (middle). At $M = 0.1$ the low-viscosity phase 1 will, where stagnant, lubricate the flow of phase 2. As for the cocurrent case, it is the low-viscosity phase that establishes the best network, both at $M = 0.1$ and $M = 10$. At $M = 10$ the wetting phase becomes immobile. As a result both the wetting and the non-wetting countercurrent relative permeabilities decrease as functions of M.

Discussion

The initial state used (random mixture of the two phases), was chosen to provide roughly history-independent relative permeabilities. It should be representative for the saturation distribution that forms when a single-phase gas experiences liquid drop-out, or when a single-phase liquid boils.

Using this approach we find that both the cocurrent and the countercurrent relative permeabilities are convex functions of saturation (convex only at intermediate saturations for the neutrally

wet cocurrent case). This convex shape is observed experimentally both in a sand pack [1] and a micromodel [9] (cocurrent, low capillary numbers), implying that the capillary forces increase with increasing interfacial area. Figure 8 (right) shows that the wetting cocurrent and countercurrent relative permeabilities are larger at a given saturation S than their non-wetting counterparts are at the saturation $1 - S$. This trend is also observed experimentally [1, 9] and indicates that a certain amount of non-wetting phase present reduces the flow of the wetting phase more than the equivalent fraction of wetting phase reduces the non-wetting flow.

We find that the cocurrent relative permeabilities increase by a factor of 2 to 2.5 when the applied force is increased by a factor 15. Thus our results are closer to those found experimentally in the micromodel [9] than those found earlier by numerical modelling [5, 6, 7]. For unit viscosity ratio, the micromodel experiments are consistent with our Fig. 13 (right) where the non-wetting relative permeability increases more than the wetting relative permeability as a function of the applied force.

Our non-wetting phase cocurrent relative permeability decreases strongly and the wetting phase cocurrent relative permeability increases weakly with increasing M. This is in conflict with the micromodel experiments [9] regarding the wetting phase. In the micromodel experiments, the capillary number $N_c = \bar{u}_1\mu_1/\sigma$ is kept constant for the various M. Using Eq. 1 it follows that $N_c = kk_{ri}F_i/\sigma$. In our investigations the applied force and the surface tension σ are kept constant, and the relative size of the capillary number is shown through k_{r1} on Fig. 17. Thus, at least some of the observed increase of k_{r1} with increasing M is probably due to the increase in N_c.

The most interesting result of the study is that the countercurrent steady state saturation distribution in general is very different from the cocurrent one. This leads to different levels of capillary influence and viscous coupling. A consequence of this is that the mobility tensor is not process independent.

Finally, it should be noted that the 2D simulation presented here does not capture everything. One important qualitative difference between 3D and 2D is that bicontinuous phases and film flow may be excluded in 2D. This study is based on the flow being driven by body-forces (such as gravity). The results may be different when flow is driven by pressure-forces instead.

Conclusions

On the basis of simulations with our simple model, we have the following conclusions:

- Both the cocurrent and the countercurrent relative permeabilities have more or less the commonly observed convex functionality with respect to saturation, see *e.g.* [1], even though our porous system is uniform.

- With increasing driving force, the cocurrent phase distribution takes the form of stationary channels aligned along the flow direction, for each phase. This reduces the capillary forces and makes the cocurrent relative permeabilities increasing functions of the applied force. For the countercurrent flow, the applied force has the tendency to mix the phases. This increases both the capillary forces and the viscous coupling, and makes the countercurrent relative permeabilities decreasing functions of the applied force.

- The viscosity ratio $M = \mu_1/\mu_2$ turns out to be important. Both the cocurrent and the countercurrent phase 2 relative permeabilities are decreasing functions of M. Except for the countercurrent phase 1-wet case, all phase 1 relative permeabilities are increasing functions of M.

- The countercurrent relative permeabilities are always less than the cocurrent ones, the difference being partly due to the opposing effect of the viscous coupling, and partly to different levels of capillary forces.

- At least at intermediate saturations, the distribution of the phases depends strongly on whether one has a cocurrent or a countercurrent flow type. Consequently, the capillary forces and the

viscous coupling are different and it seems that the general mobility tensor in Eq. 2 is process-dependent, and cannot cover both cocurrent and countercurrent flow.

Acknowledgments

This work has received support from the Research Council of Norway (PROPETRO and the Programme for Supercomputing) through a PhD-grant (K.L.) and through a subvention of computing time on the Origin 2000 at Parallab, Bergen.

References

[1] Bentsen, R.G., Manai, A.A., "On the use of conventional cocurrent and countercurrent effective permeabilities to estimate the four generalized permeability coefficients which arise in coupled, two-phase flow", *Transport in Porous Media*, (1993) **11**, 243–262.

[2] Bear, J., *Dynamics of Fluids in Porous Media*, Elsevier, New York, (1972).

[3] De Gennes, P.G., "Theory of slow biphasic flows in porous media", *PCH PhysicoChemical Hydrodynamics*, (1983) **4**, 178–185.

[4] Kalaydjian, F., "A macroscopic description of multiphase flow in porous media involving space-time evolution of fluid/fluid interface", *Transport in Porous Media*, (1987) **2**, 537–552.

[5] Rothman, D.H., "Macroscopic laws for immiscible two-phase flow in porous media: Results from numerical experiments", *Journal of Geophysical Research*, (1990) **95**, 8663–8674.

[6] Gunstensen, A.K., Rothman, D.H., "Lattice-boltzmann studies of immiscible two-phase flow through porous media" *Journal of Geophysical Research*, (1993) **98**, 6431–6441.

[7] Olson, J.F., Rothman, D.H., "Two-fluid flow in sedimentary rock: Simulation, transport and compexity", *J. Fluid Mech.*, (1997) **341**, 343–370.

[8] Avraam, D.G., Payatakes, A.C., "Generalized relative permeability coefficients during steady-state two-phase flow in porous media, and correlation with the flow mechanisms", *Transport in Porous Media*, (1995) **20**, 135–168.

[9] Avraam, D.G., Payatakes, A.C., "Flow regimes and relative permeabilities during steady-state two-phase flow in porous media", *J. Fluid Mech.*, (1995) **293**, 207–236.

[10] Goode, P.A., Ramakrishnan, T.S., "Momentum transfer across fluid-fluid interfaces in porous media: A network model", *AIChE Journal*, (1993) **39**, 1124–1134.

[11] Odeh, A.S., "Effect of viscosity ratio on relative permeability", *J. Pet. Tech.*, (1959) **216**, 346–353.

[12] Orlandini, E., Swift, M.R., Yeomans, J.M., "A lattice boltzmann model of binary-fluid mixtures", *Europhys. Lett.*, (1995) **32**, 463–468.

[13] Swift, M.R., Orlandini, E., Osborn, W.R., Yeomans, J.M., "Lattice boltzmann simulations of liquid-gas and binary fluid systems", *Phys. Rev. E*, (1996) **54**, 5041–5052.

[14] Langaas, K., Yeomans, J.M., "Lattice boltzmann simulations of a binary fluid with different phase viscosities and its application to fingering in two dimensions", *Preprint*, (1998).

[15] Langaas, K., Grubert, D., "Lattice boltzmann simulations of wetting and dpr gel", In *Proceedings from the 5'th International Symposium on Evaluation of Reservoir Wettability and its Effect on Oil Recovery, 22-24 June 1998*, (1998).

[16] Wagner, A., *Theory and applications of the lattice Boltzmann method*, PhD thesis, University of Oxford, (1997).

[17] Langaas, K., "Viscous coupling and two-phase flow in porous media", In *Proceedings from the 6'th European Conference on the Mathematics of Oil Recovery, 8-11 Sept. 1998*, EAGE, Houten (1998).

[18] Forchheimer, P., "Wasserbewegnung durch boden", *Z. d. V. deutch. Ing.*, (1901) **45**, 1781–1788.

Figures

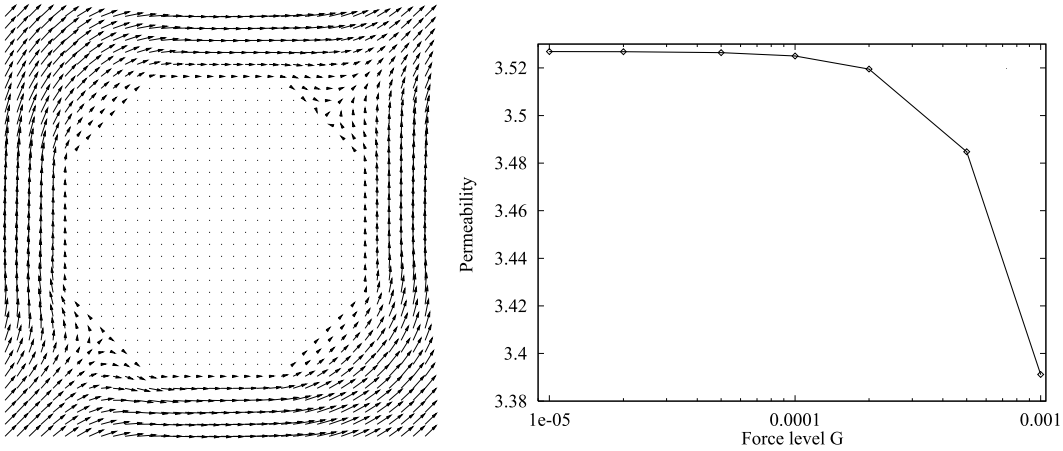

Figure 1: Single-phase flow. Steady state velocity field (left) and permeability as a function of forcing level (right).

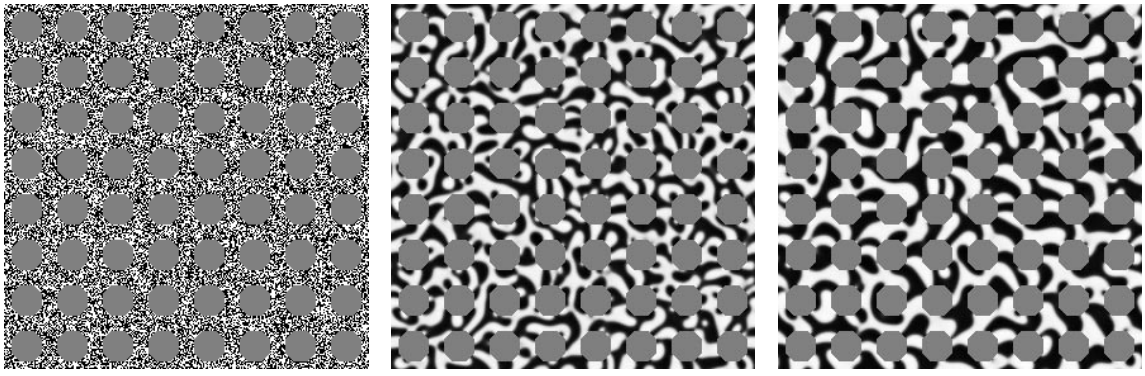

Figure 2: Two-phase flow in neutrally wet system. Phase distribution at time step 0 (left), time step 1000 (middle) and time step 2000 (right). $G = 10^{-4}$, $M = 1$.

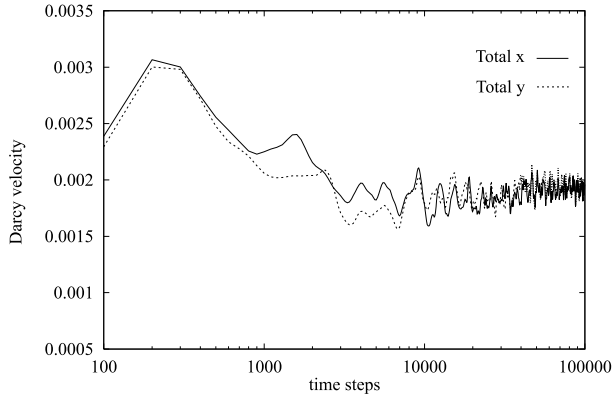

Figure 3: Two-phase flow in neutrally wet system. Average velocities as a function of time.

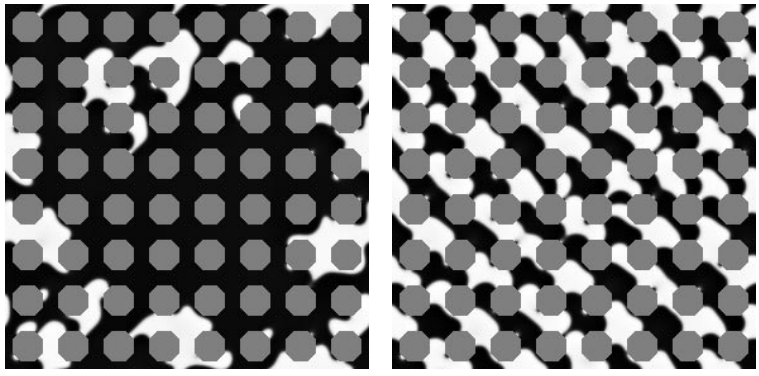

Figure 4: Steady state cocurrent flow. Neutral wettability. Saturation of phase 1 is 0.25 (left) and 0.5 (right). $G = 10^{-4}$, $M = 1$.

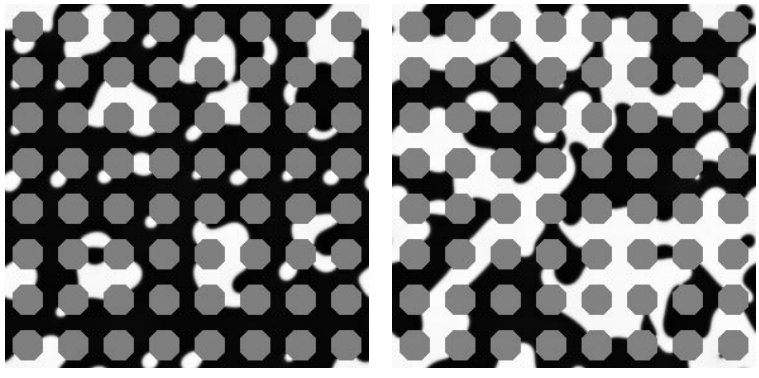

Figure 5: Steady state countercurrent flow. Neutral wettability. Saturation of phase 1 is 0.25 (left) and 0.5 (right). $G = 10^{-4}$, $M = 1$.

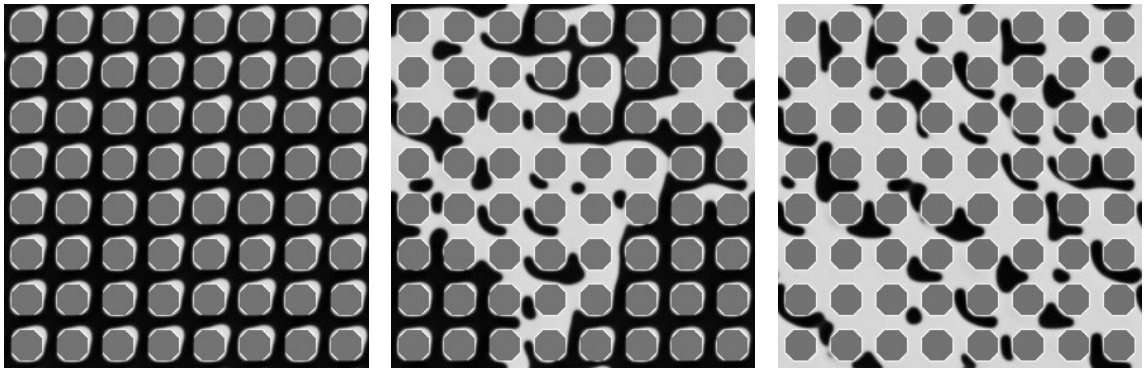

Figure 6: Steady state cocurrent flow. Phase 1-wet system. Saturation of phase 1 is 0.25 (left), 0.5 (middle) and 0.75 (right). $G = 10^{-4}$, $M = 1$.

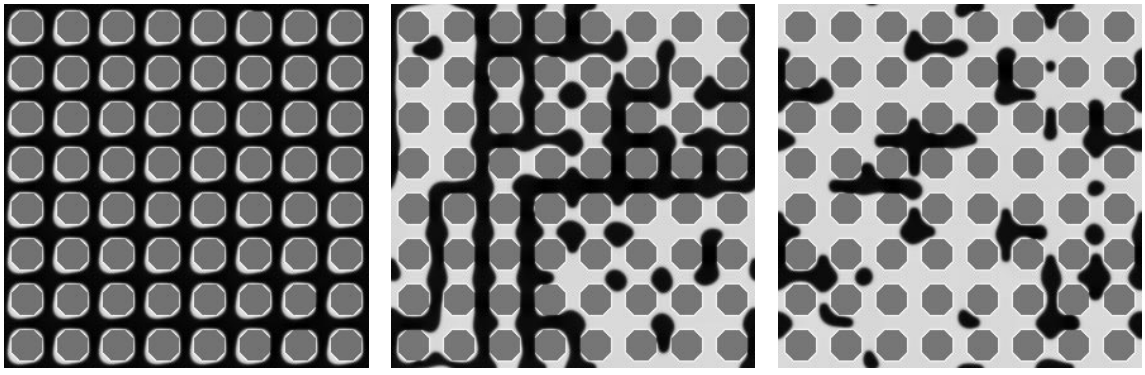

Figure 7: Steady state countercurrent flow. Phase 1-wet system. Saturation of phase 1 is 0.25 (left), 0.5 (middle) and 0.75 (right). $G = 10^{-4}$, $M = 1$.

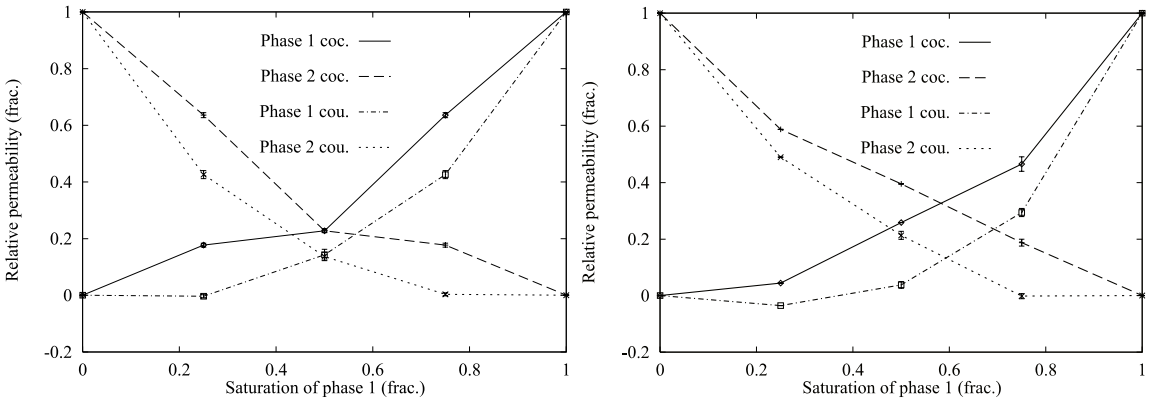

Figure 8: Steady state cocurrent (coc.) and countercurrent (cou.) relative permeabilities as functions of phase 1 saturation. Neutral wet (left) and phase 1-wet system (right). The error bars indicate standard deviations (one above, one below) for each steady state. $G = 10^{-4}$, $M = 1$.

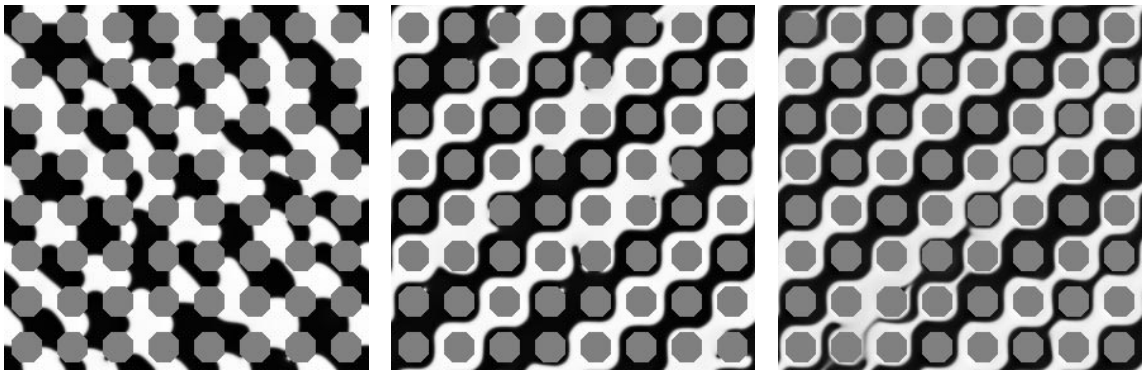

Figure 9: Steady state cocurrent flow. Neutral wettability. Level of forcing (G) is $5\,10^{-5}$ (left), $2\,10^{-4}$ (middle), and 10^{-3} (right). $S = 0.5$, $M = 1$.

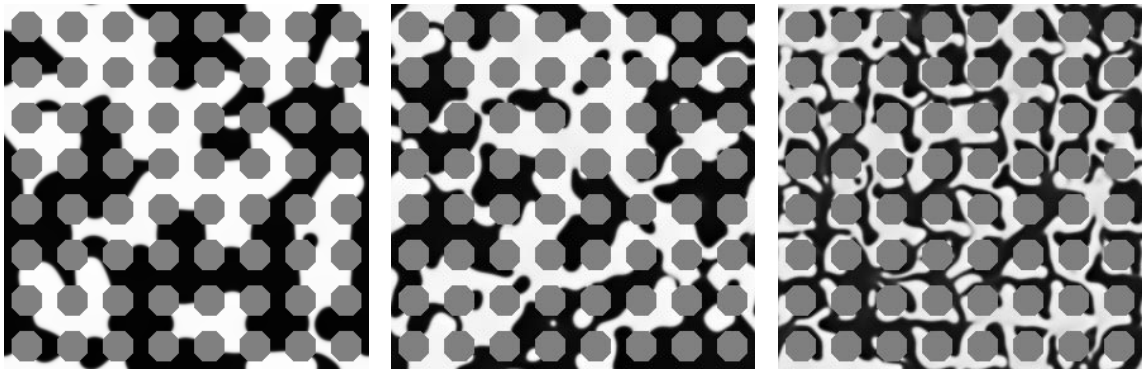

Figure 10: Steady state countercurrent flow. Neutral wettability. Level of forcing (G) is $5\,10^{-5}$ (left), $2\,10^{-4}$ (middle), and 10^{-3} (right). $S = 0.5$, $M = 1$.

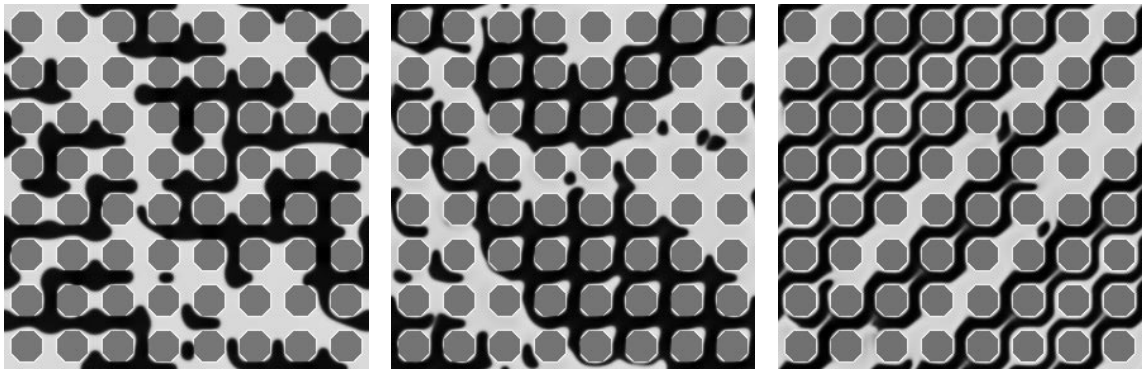

Figure 11: Steady state cocurrent flow. Phase 1-wet system. Level of forcing (G) is $5\,10^{-5}$ (left), $2\,10^{-4}$ (middle), and $5\,10^{-4}$ (right). $S = 0.5$, $M = 1$.

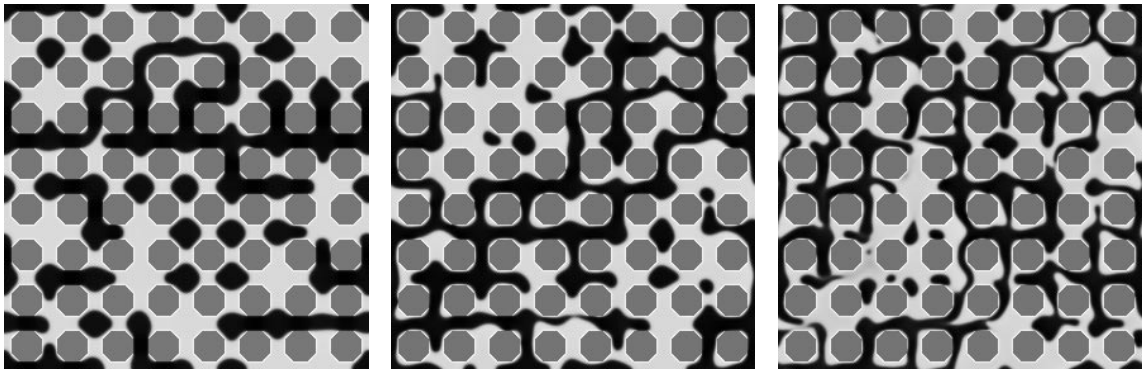

Figure 12: Steady state countercurrent flow. Phase 1-wet system. Level of forcing (G) is $5\,10^{-5}$ (left), $2\,10^{-4}$ (middle), and $5\,10^{-4}$ (right). $S = 0.5$, $M = 1$.

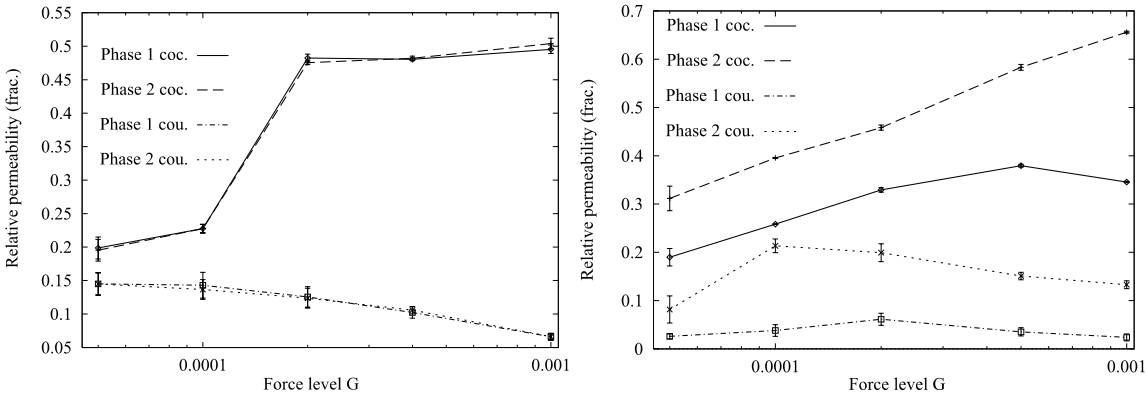

Figure 13: Steady state cocurrent (coc.) and countercurrent (cou.) relative permeabilities as functions of forcing level (G). Neutrally wet (left) and phase 1-wet system (right). $S = 0.5$, $M = 1$.

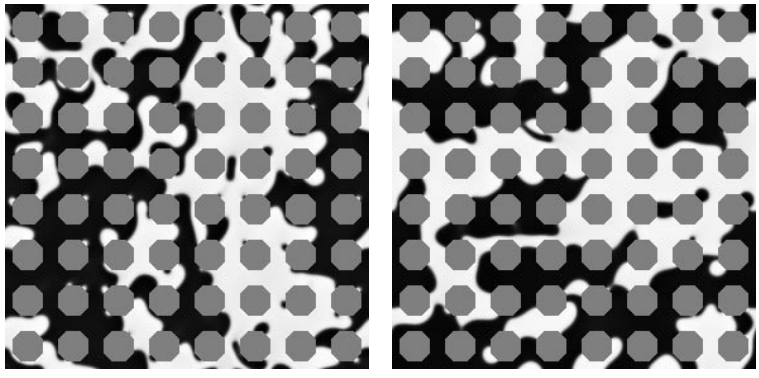

Figure 14: Steady state flow in a neutrally wet system. Viscosity ratio (M) is 0.1. cocurrent (left) and countercurrent (right). $G = 10^{-4}$, $S = 0.5$.

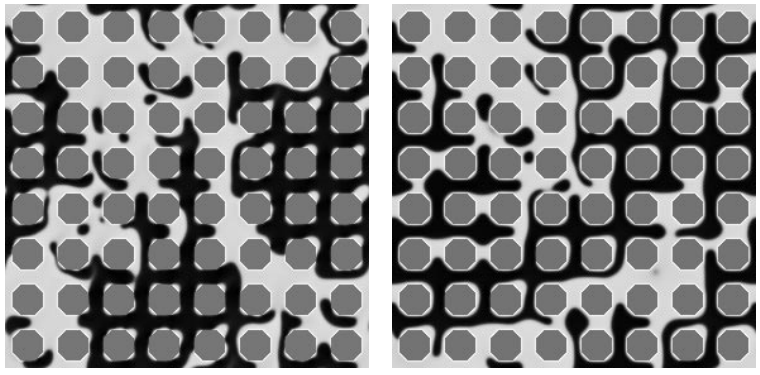

Figure 15: Steady state cocurrent flow in a phase 1-wet system. Viscosity ratio (M) is 0.1 (left) and 10 (right). $G = 10^{-4}$, $S = 0.5$.

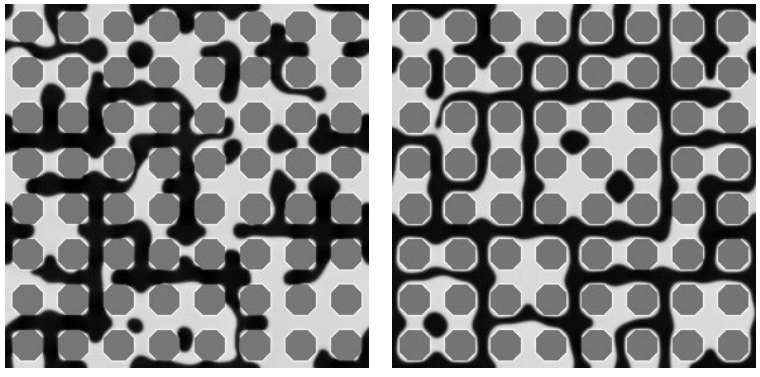

Figure 16: Steady state countercurrent flow in a phase 1-wet system. Viscosity ratio (M) is 0.1 (left) and 10 (right). $G = 10^{-4}$, $S = 0.5$.

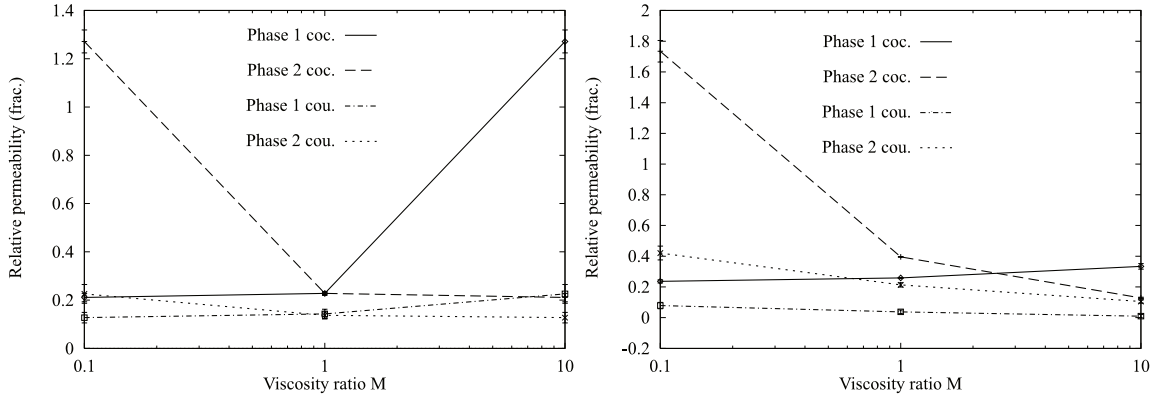

Figure 17: Steady state cocurrent (coc.) and countercurrent (cou.) relative permeabilities as functions of the viscosity ratio (M). Neutrally wet (left) and phase 1-wet system (right). $G = 10^{-4}$, $S = 0.5$.